



An Optimized and Advanced Algorithm for the Quantification of Immunohistochemical Biomarkers in Keratinocytes

Lindsey G. Siegfried¹, Sophie M. Bilik¹, Jamie L. Burgess¹, Paola Catanuto¹, Ivan Jozic¹, Irena Pastar¹, Rivka C. Stone^{1,2} and Marjana Tomic-Canic^{1,2}

Advancements in pathology have given rise to software applications intended to minimize human error and improve efficacy of image analysis. Still, the subjectivity of image quantification performed manually and the limitations of the most ubiquitous tissue stain analysis software requiring parameters tuned by the observer, reveal the need for a highly accurate, automated nuclear quantification software specific to immunohistochemistry, with improved precision and efficiency compared with the methods currently in use. We present a method for the quantification of immunohistochemical biomarkers in keratinocyte nuclei proposed to overcome these limitations, contributing sensitive shape-focused segmentation, accurate nuclear detection, and automated device-independent color assessment, without observer-dependent analysis parameters.

Keywords: Automated digital pathology, Biomarker, Epidermal structures, Immunohistochemistry, Quantification

JID Innovations (2024);4:100270 doi:10.1016/j.xjidi.2024.100270

INTRODUCTION

Immunohistochemistry (IHC) has widespread usage for reliable, cost-effective protein expression visualization and analysis in clinical diagnostics as well as biomarker research. The fundamental chemistry of IHC is based on the deposition of a chromogen such as diaminobenzidine (DAB) in the location of an antigen–antibody complex on slide-mounted tissue sections, producing pigmentation in the areas where a protein of interest is expressed (Sukswai and Khoury, 2019). The evolution of IHC from diagnostic to prognostic biomarker analysis has created a demand for stain quantification. However, traditional manual assessment by a pathologist is impractical owing to the volume of images required (Taylor and Levenson, 2006). Thus, we developed a Standardized

Algorithm for Nuclear DAB Detection (SANDD) to improve quantification accuracy compared with that of images evaluated by existing methods.

Digital pathology, facilitated by the increasing interest in biomarker data and the prevalence of digital slide imaging, presents many challenges despite great promise. The potential that fully automated, unsupervised, artificial intelligence–based image assessment looms on the horizon is built on contributions to computational pathology dating as early as 1965 (Madabhushi and Lee, 2016; Mendelsohn et al, 1965). In the past decades, numerous approaches to IHC and other tissue image quantification have been detailed in the literature, each presenting contributions although subject to common caveats and pitfalls (Akakin et al, 2015). Approaches detailed in the literature predominantly focus on specific protein expression in limited cell or tissue types owing to the complexity of histologic structures (Chen et al, 2019; Fernández-Carrobles et al, 2017; Valdebran et al, 2020). Development of deep learning neural networks in tissue image analysis is an ongoing area of research, with the aim of broad application and assessment superior to the eye of a pathologist (Seo et al, 2020; Wang et al, 2019).

The quirks of IHC notoriously result in intra- and interbatch variability due to a combination of factors, and additional aspects contribute to the difficulty of accurate nuclear segmentation. This is attributable in part to the unpredictable effects of the process of pathology preparation, tissue heterogeneity, and variations in imaging conditions (Cregger et al, 2006; Di Cataldo et al, 2010). IHC variability and approaches for standardizing preanalytic methods for the stain itself are reviewed elsewhere but nonetheless are necessary to address, especially in biomarker validation trials (Anagnostou et al, 2010; Elliott et al, 2015; Engel and Moore, 2011; Grube, 2004; Guedes et al, 2019; Janardhan et al, 2018; Libard et al, 2019).

¹Wound Healing and Regenerative Medicine Research Program, Dr. Philip Frost Department of Dermatology and Cutaneous Surgery, University of Miami Miller School of Medicine, Miami, Florida, USA

²These authors contributed equally to this work.

Correspondence: Rivka C. Stone, Dr. Philip Frost Department of Dermatology and Cutaneous Surgery, University of Miami Miller School of Medicine, 600 Northwest 10th Avenue, Rosenstiel Medical Science Building 2023A, Miami, Florida 33136, USA. E-mail: rivka.stone@med.miami.edu and Marjana Tomic-Canic, Dr. Philip Frost Department of Dermatology and Cutaneous Surgery, University of Miami Miller School of Medicine, 1600 Northwest 10th Avenue, Rosenstiel Medical Science Building 2023A, Miami, Florida 33136, USA. E-mail: mtcanic@med.miami.edu

Abbreviations: CV, coefficient of variation; DAB, diaminobenzidine; DFU, diabetic foot ulcer; FFPE, formalin-fixed paraffin-embedded; GPU, graphics processing unit; IDE, integrated development environment; IHC, immunohistochemistry; PC, personal computer; pGR, phosphorylated glucocorticoid receptor; RGB, red, green, and blue; SANDD, Standardized Algorithm for Nuclear Diaminobenzidine Detection; TMA, tissue microarray

Received 31 July 2023; revised 10 January 2024; accepted 12 January 2024

Cite this article as: *JID Innovations* 2024;4:100270

Previously published literature on digital pathology image analysis is based on IHC of tissue microarray (TMA), especially in cancer diagnostics and research. Automated segmentation of TMA images is a more efficient process than whole-section segmentation because the regions or cores are small, defined shapes with few nuclei compared to the original paraffin-embedded sample from which the cores are taken. When sections of formalin-fixed paraffin-embedded (FFPE) human skin are evaluated as biopsies in their entirety rather than small regions of interest within a biopsy section, image segmentation challenges generally unique to skin arise owing to the nature of skin layers. Although automated segmentation of keratinocyte nuclei from the cytoplasm is straightforward, as detailed here, the separation of epidermal and dermal compartments within an image remains best performed by a human observer. Recent attempts to segment the epidermis and dermis in low-magnification hematoxylin and eosin (H&E) FFPE sections have been successful, although the contrast between dermis and epidermis is more visually apparent on H&E than on hematoxylin and DAB stain (Xu and Mandal, 2015).

Comparison with other methods

ImageJ plugins have been developed for cell counting and stain scoring of IHC, although few protocols have been detailed in the literature with sufficient information for reproducibility (Crowe and Yue, 2019; Varghese et al, 2014). ImageJ and its associated plugins are freely available from the National Institutes of Health, making it an attractive approach to researchers (Schneider et al, 2012). However, they require subjective human input such as setting background color thresholds. To minimize the time-consuming nature of some of these approaches, groups may divide the analysis across multiple observers and thus introduce a significant amount of bias and interobserver variability.

The most widely used open-source software available to perform nuclear stain quantification is QuPath (Bankhead et al, 2017). QuPath provides myriad algorithms for tissue image processing and whole-slide imaging in a graphical user interface as well as the ability to execute user-designed scripts. The contributions of QuPath to digital pathology are globally extensive, and it is the framework of choice for researchers for a multitude of applications (Humphries et al, 2021).

However, the literature lacks detailed and user-friendly protocols for users without considerable mathematical and computing backgrounds. As with ImageJ, substantial amounts of subjective decision making are required to set color and segmentation thresholds as well as annotations of specific regions (Table 1). Manual removal of problematic areas on images or slides or TMA can also be necessary when using QuPath (Morriss et al, 2020). Again, similar to the ImageJ approaches, analysis by 1 observer may be consistent, but the introduction of multiple observers diminishes consistency. Initial attempts to quantify IHC staining of biomarkers of interest in the epidermis of whole human skin sections across multiple users in our group using QuPath yielded not only unacceptable variability between observers (Table 2 and Figure 1) but also inaccurate cell detection (Figure 2), revealing the need for an improved workflow for accurate nuclear detection and objective color assessment.

Table 1. Advantages and Disadvantages of Common Digital Pathology Methods for Quantifying IHC Staining

Approach	Advantages	Disadvantages
ImageJ (plugins IHC Profiler, ImmunoRatio)	Free, open access Multiple applications documented in the literature Ongoing third-party plugin development	Extensive user interaction Expertise required to operate effectively Lack of detailed protocols
QuPath	Broad functionality Widespread use	Extensive user interaction Error rate Expertise required to operate effectively
SANDD	Ease of use No user-defined thresholds Improved accuracy over other methods Handling of large images	Only applied to keratinocytes Specific to nuclear staining Region of interest selected by the user

Abbreviations: IHC, immunohistochemistry; SANDD, Standardized Algorithm for Nuclear Diaminobenzidine Detection.

RESULTS

Development of SANDD

This program utilizes the OpenCV (Open Computer Vision) library (version 4.5.5), a library of functions for image processing, and was written and run in Python 3.9.12. Upon running, an image is imported using OpenCV standard blue, green, and red color space; converted to red, green, and blue (RGB); and stored in grayscale and L*a*b* conversions.

Scales such as RGB and cyan, magenta, yellow, and key (CMYK) are used to describe color. The CIELAB (L*a*b*) color space expresses color in 3 dimensions: L*, with 0 representing black and 100 representing white; a*, with negative values representing green and positive values representing red; and b*, with negative values representing blue and positive values representing yellow (Figure 3). Unlike RGB, this color space is device independent and is validated for quantifying color in multiple industries. The standard illuminant or white point may vary from industry to industry, although this application uses the recommended International Commission on Illumination standard illuminant D65 for this color space, which approximates mid-day light with a clear sky in Western Europe (Fullerton et al, 1996). Conversion of RGB images to L*a*b* is rapidly performed by the OpenCV cvtColor() function and no longer possesses the time-consuming constraints of color space conversion previously required (Bradski, 2000; Connolly and Fleiss, 1997).

Image thresholding is a commonly used process to identify shapes and characters within an image and produces a binary segmented image containing a background in black and objects in white. Depending on the application, different approaches for thresholding or binarization may be appropriate. Given the variable color and intensity landscape of tissue sections, applying a universal threshold leads to inadequate binarization—a more sensitive threshold may register areas of noise as nuclei, and a less sensitive threshold may not register light-colored nuclei with less intense staining. Varying distances between nuclei and varying nuclear

Table 2. Comparison of QuPath with SANDD Total and Positive Nuclei Counts of Keratinocytes Stained for c-Myc in the Same Set of 5 Images, Quantified by 4 Observers

Image	User	QuPath			SANDD			CV (QuPath)	CV (SANDD)
		Total Nuclei (Count)	Positive Nuclei (Count)	Positive Nuclei (%)	Total Nuclei (Count)	Positive Nuclei (Count)	Positive Nuclei (%)		
Image #1	1	3216	2792	86.82	3943	2921	74.08	23.23	1.549
	2	4103	2145	52.28	3971	2910	73.28		
	3	1838	1583	86.13	3347	2430	72.60		
	4	2406	2242	93.18	3424	2577	75.26		
Image #2	1	7105	4532	63.79	6830	4764	69.75	26.75	1.879
	2	7788	3974	51.03	5993	4255	71.00		
	3	7207	4252	59.00	5741	4100	71.42		
	4	3497	3213	91.88	5518	3780	68.50		
Image #3	1	5982	4229	70.70	6381	4698	73.62	34.96	3.154
	2	6914	2541	36.75	5186	4057	78.23		
	3	2069	1611	77.86	4959	3914	78.93		
	4	3235	3080	95.21	4754	3716	78.17		
Image #4	1	4703	3897	82.86	4758	2487	52.27	22.33	3.05
	2	2853	1562	54.75	4237	2295	54.17		
	3	4942	2913	58.94	3234	1676	51.82		
	4	2910	2469	84.85	3836	1930	50.31		
Image #5	1	2844	2051	72.12	4051	1807	44.61	27.88	4.923
	2	3086	1126	36.49	3789	1740	45.92		
	3	2862	1599	55.87	3218	1609	50.00		
	4	1773	1232	69.49	3488	1622	46.50		

Abbreviations: #, number; CV, coefficient of variation; SANDD, Standardized Algorithm for Nuclear Diaminobenzidine Detection. CV is calculated across observer measurements of percentage positive nuclei.

morphology resulting from normal keratinocyte differentiation make skin biopsies susceptible to oversegmentation that is common with techniques such as the watershed algorithm that separates objects from an image on the basis of the

definite foreground and background of the entire image (Di Cataldo et al, 2010). Segmentation using partitions or sub-regions proportional to the image size was selected for adaptability and more precise handling using the OpenCV

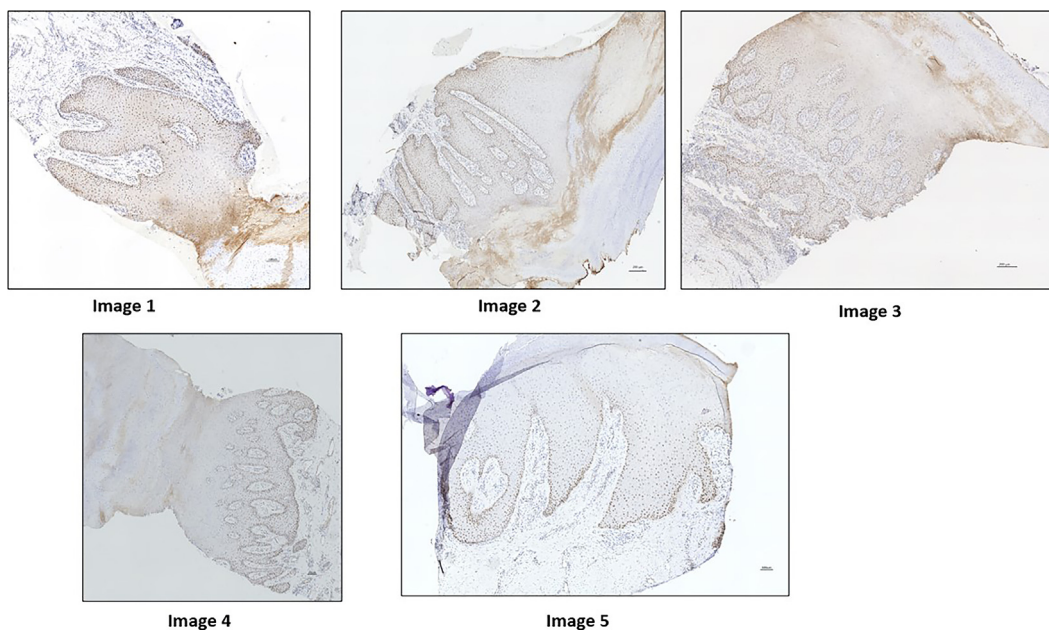


Figure 1. Corresponding set of images from 5 DFUs analyzed by QuPath and SANDD to obtain total and positive nuclei counts. These images are referenced in Figure 10 and Table 2. Bar = 100 μ m. DFU, diabetic foot ulcer; SANDD, Standardized Algorithm for Nuclear Diaminobenzidine Detection.

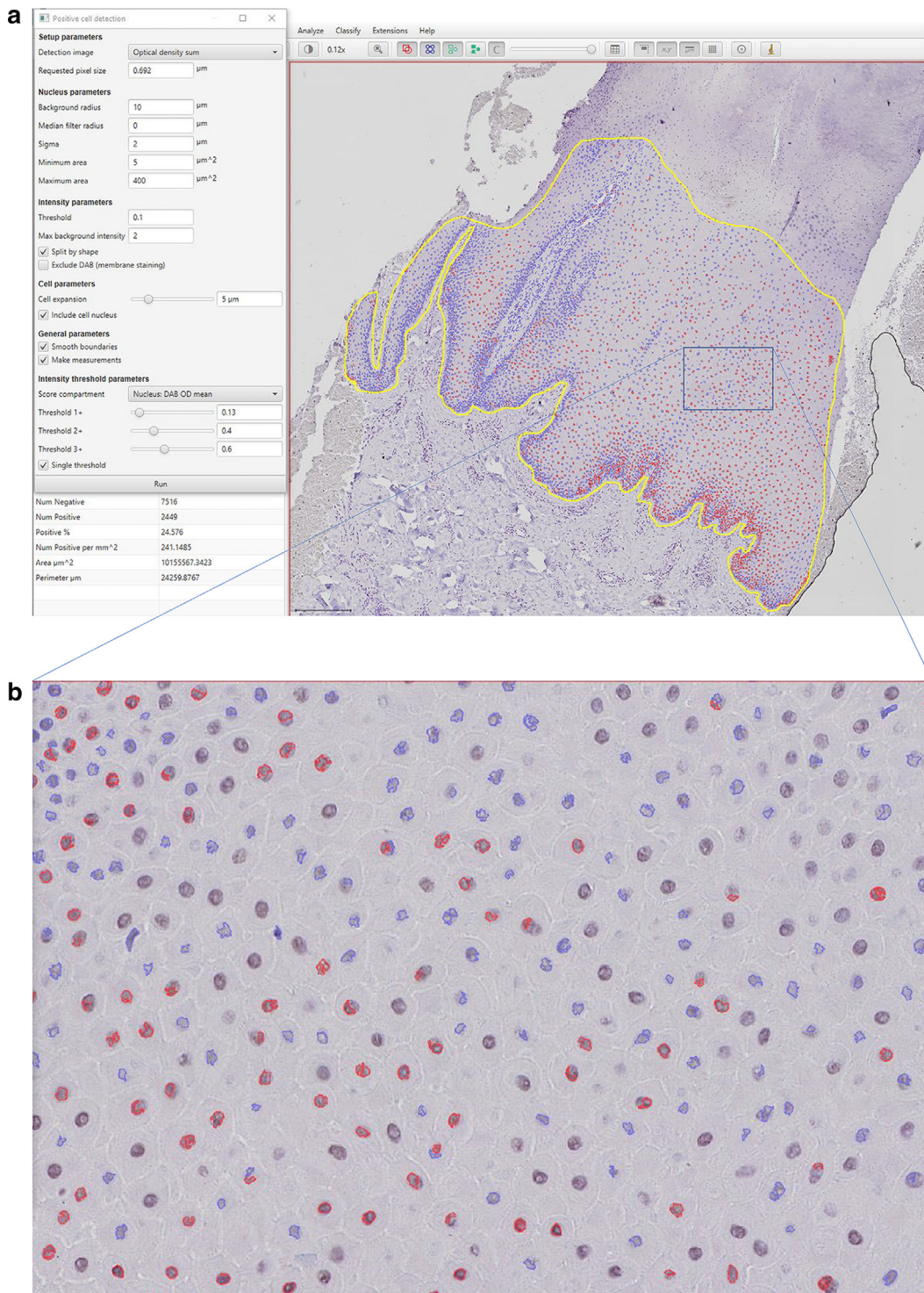


Figure 2. Results from positive cell detection function in QuPath. (a) QuPath interface with nuclei detected and user-defined settings for positive nuclei. **(b)** Portion of the region of interest showing uncounted nuclei (lacking a red or blue outline) as well as individual nuclei detected as multiple fragments. Bar = 100 µm.

function `adaptiveThreshold()`. Testing of various partitions per image relative to whole image size yielded the cleanest and most accurate thresholding at 125,000 partitions per image.

Once nuclei are separated from the cytoplasm to produce a binary image, a series of morphological transformations in the OpenCV library such as `morph.close()` and `morph.erode()` are performed to separate densely packed nuclei and clearly define nuclear edges. Within the OpenCV library, the contour

detection function `findContours()` was selected as the most appropriate for keratinocyte nuclear shape detection. The boundaries of the nuclei are detected and stored as coordinates using `drawContours()`, and a binary mask of each nucleus is generated to produce a list of coordinates of all pixels within the boundary. Iterating pixel-by-pixel, contour-by-contour, the whole image in $L^*a^*b^*$ color space is referenced. The approach of averaging nucleus color is more

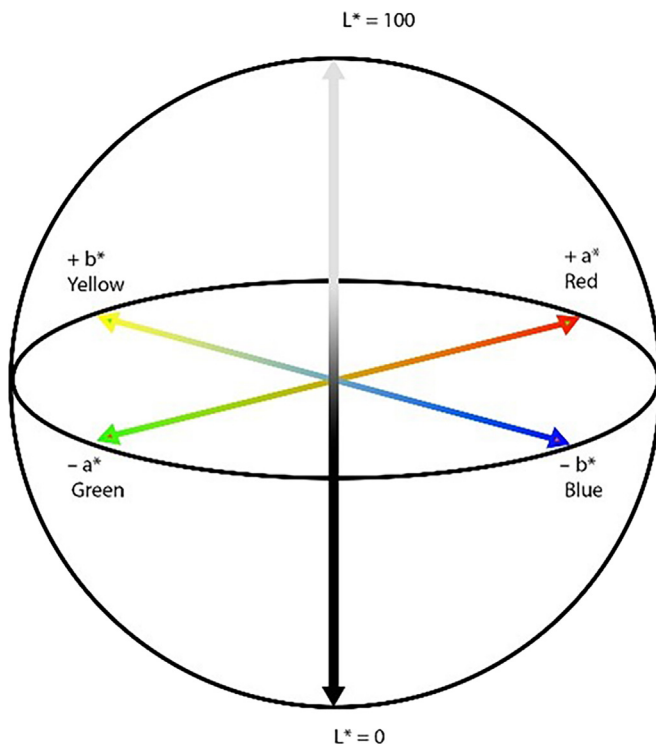


Figure 3. Three-dimensional representation of the $L^*a^*b^*$ color space.

efficient with respect to runtime and memory; however, the need for utmost precision dictates that the data loss that occurs when averaging over areas outweighs the efficiency advantage. Nuclei often do not stain evenly and possess areas of brown and blue concurrently, also a factor in interobserver variability.

The ratio of red to blue and presence of yellow are used to determine a positive, DAB-stained pixel. In applications where DAB staining remains exclusively nuclear and does not generate cytoplasmic stain, the average cytoplasmic color can be used as a reference point to normalize for sections with low-contrast overall staining or to account for sections with nonspecific staining throughout. If the ratio of red to blue and the presence of yellow within the pixel indicates brownness, it is set to positive. A ratio of 40% positive pixels within a nucleus designates the whole nucleus as positive. Setting a minimum pixel percent positive per nucleus threshold eliminates the need for the commonly used user-defined threshold with respect to the entire image and/or its associated negative control. Size constraints remove nuclei below the 5th and above the 95th percentiles to avoid the implementation of a universal size constraint. These procedures are depicted graphically in Figure 4.

The program returns values for total, positive, and negative nuclei as well as images corresponding to each stage of the segmentation, cleanup, and detection processes for quality control (Figure 5). The final image generated contains positive nuclei indicated by a red outline and negative nuclei indicated by a blue outline.

Anticipated results

This protocol generates numeric data for the counts of total, positive, and negative nuclei detected in IHC staining images

as well as TIFF images for visualization and quality control along the program pipeline (Table 2 and Figure 1). Results will be unchanged when rerunning the program if the image and the code parameters are unchanged. The numeric data produced by this protocol allows for a quantitative comparison of nuclear biomarker expression between human skin samples.

The application emphasized in the creation of this protocol was the prognostic implications of skin biopsy staining positivity relative to a hypothesized threshold. The data generated by this protocol demonstrated that segmentation of epidermal keratinocytes in diabetic foot ulcer (DFU) biopsy and debridement tissue using SANDD yielded more accurate nuclear shape detection than using QuPath (Figure 6). Implementation of this protocol in analyzing murine and porcine skin samples demonstrated future applicability in animal studies (Figures 7, 8, and 9). In addition, the coefficient of variation (CV) between nuclei measurements from multiple users independently quantifying the same set of images was significantly lower when using SANDD than when using QuPath (Figures 1 and 10 and Table 2).

DISCUSSION AND POTENTIAL APPLICATIONS

Application of the protocol to nuclear c-Myc quantification in keratinocytes

Activation of c-Myc in chronic wounds such as DFUs is associated with a hyperproliferative, nonmigratory epidermis that is incompatible with healing (Sawaya et al, 2018; Stojadinovic et al, 2005). Quantitative c-Myc expression in keratinocytes from biopsies or debridement tissue of DFUs is proposed as a biomarker for healing prognosis. Phosphorylated glucocorticoid receptor (pGR) is also proposed to contribute to persistence of the nonhealing chronic wound phenotype (Stojadinovic et al, 2007).

Tissue from the wound edge of DFUs at weeks 1 and 5 of study enrollment underwent routine processing for paraffin embedding, and sections were subsequently stained for both c-Myc and pGR. Imaging was performed on (Keyence slide scanner) at $\times 20$ magnification. Initial quantification of c-Myc and pGR expression using the positive cell detection feature in QuPath yielded the results mentioned earlier (Figure 10), eventually leading to the development of this protocol.

Application of the protocol to nonhuman epidermal biomarker quantification

To further demonstrate the potential uses of SANDD, we evaluated IHC-stained animal skin as well. Porcine and murine skin, among other common model species, share epidermal characteristics and can be analyzed using this method. Staining for phosphorylated c-Jun in both porcine skin (Figure 11) and murine skin (Figure 7) affirmed that the epidermal morphology similarities to human skin allow for SANDD-based biomarker analysis. Comparison of QuPath performance with that of SANDD in murine and porcine skin showed similar improvements in detection of nuclei and in counts of positively stained nuclei (Figures 8 and 9 and Table 3).

Limitations

The requirement to predefine the epidermis or epidermal region of interest can be time consuming in a high-throughput

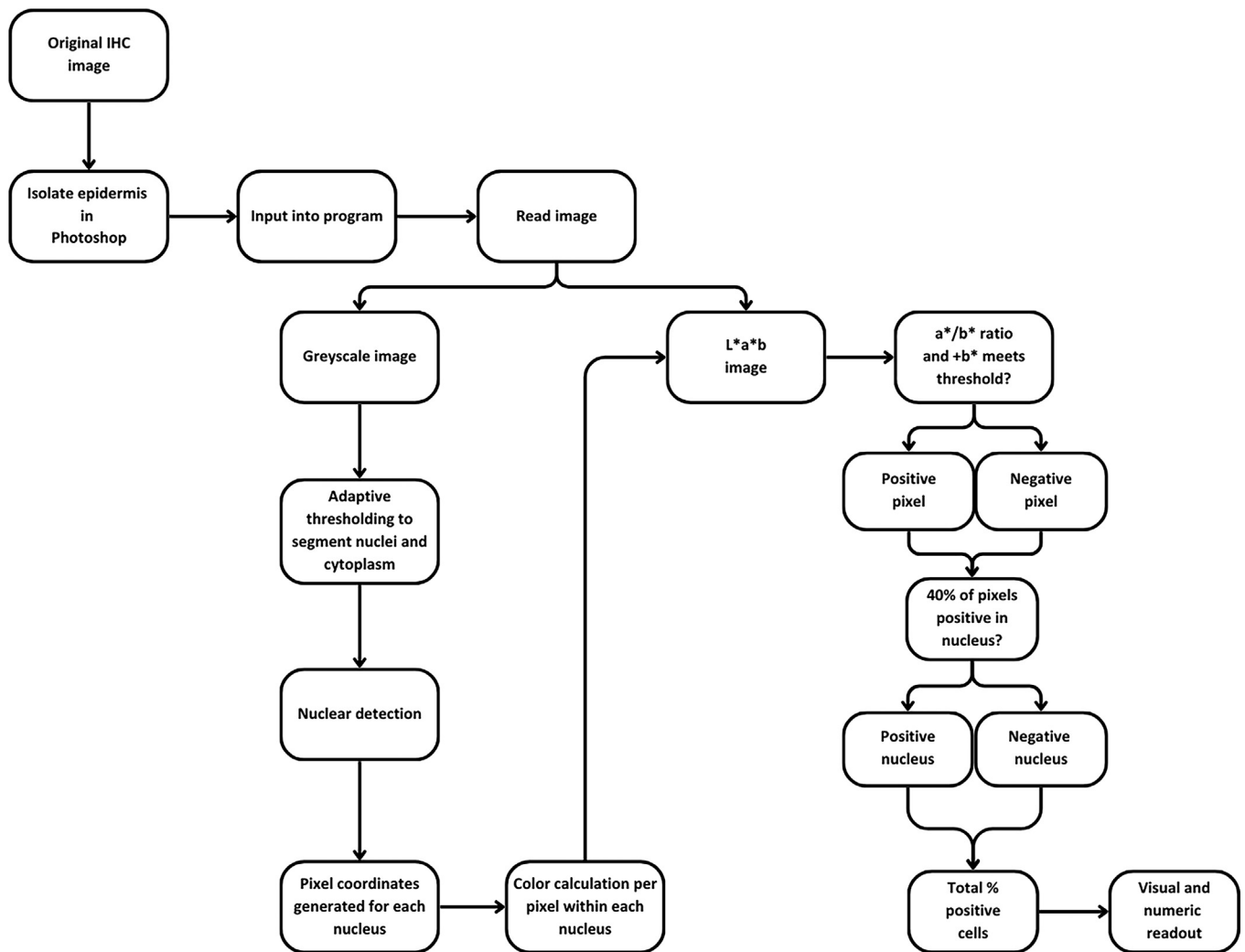


Figure 4. Flowchart demonstrating the steps of the SANDD process. IHC, immunohistochemistry; SANDD, Standardized Algorithm for Nuclear Diaminobenzidine Detection.

endeavor. Although the user-defined area of a whole-skin section is more representative of the tissue than TMA, and a minimum number of nuclei is suggested to maintain as representative an image as possible, subjective decision making is required to define the region of interest. Future directions should focus on efficient computer-automated identification of skin anatomy in high-magnification IHC images to continue to reduce subjectivity and potential bias.

MATERIALS AND METHODS

Expertise needed to implement the protocol

For the application mentioned earlier, this program can be implemented without specialized coding or computational expertise. If project-specific modifications are necessary, a user competent in Python coding should perform them. Users with basic coding knowledge or familiarity with Python will find the simple, readable structure of the source code manageable.

Timing

After IHC staining and microscopy, the preprocessing of each image takes approximately 10 minutes. Images tested were taken at $\times 20$ magnification, ranged in size from 50 to 500 mb each, and had widths and heights between 2000 and 7000 pixels. The reported

runtime per image ranged from 4 to 10 minutes depending on the size of the image. Runtime is expected to vary on the basis of the specifications of the computer; thus, it is anticipated that even higher-performance computing power will reduce the runtime. The advantage of a device-independent and uniform color space such as L*a*b* allows users to maximize speed using multiple computers to run the program.

Statistical methods

For each image analyzed by QuPath versus SANDD, mean, SD, and CV (calculated as SD divided by mean) were determined for nuclei measurements across observers. Shapiro–Wilk test was used to confirm normal distribution of nuclei measurements and CVs. Two-tailed paired *t*-test was used to detect differences between QuPath and SANDD quantifications by image, with significance at $P < .05$.

Equipment needed

The following equipment are needed:

1. A computer: This program was developed and run on a Dell. Personal computer (PC) with an 11th-generation Intel Core i7-11700 central processing unit (CPU), 512 GB PM9A1 NVMe

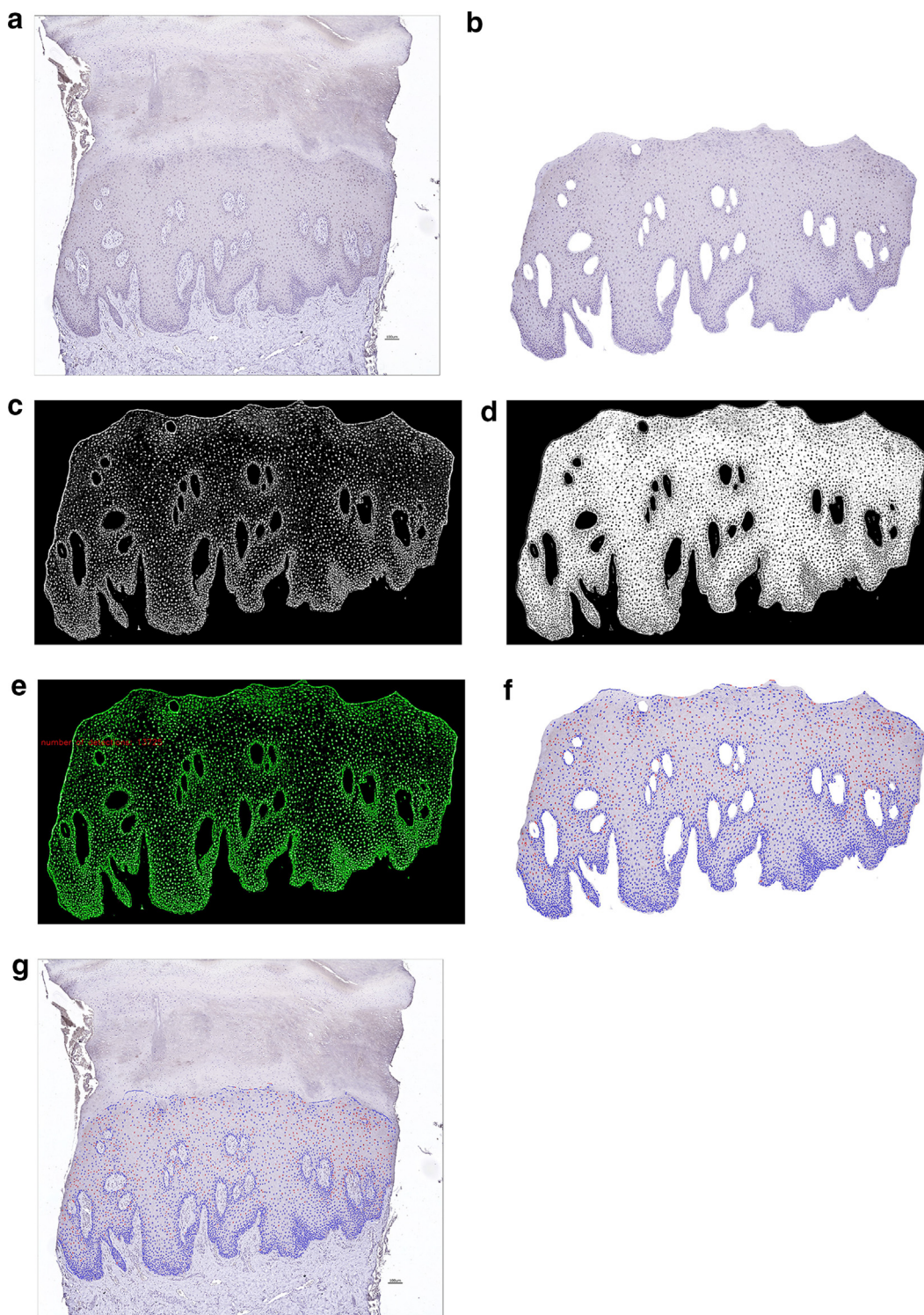


Figure 5. Image processing workflow in SANDD. (a) Original image of IHC-stained skin biopsy for phosphorylated glucocorticoid receptor. (b) Image after preprocessing in Photoshop to isolate epidermis. (c) Binary image after thresholding and segmentation. Nuclei are in white. (d) Binary image after thresholding and segmentation. Cytoplasm is in white. (e) Result of nucleus detection. Detections are outlined in green. (f) Final image output with positive nuclei outlined in red and negative nuclei outlined in blue. (g) Final image composited with original whole-section image. Bar = 100 μ m. IHC, immunohistochemistry; SANDD, Standardized Algorithm for Nuclear Diaminobenzidine Detection.

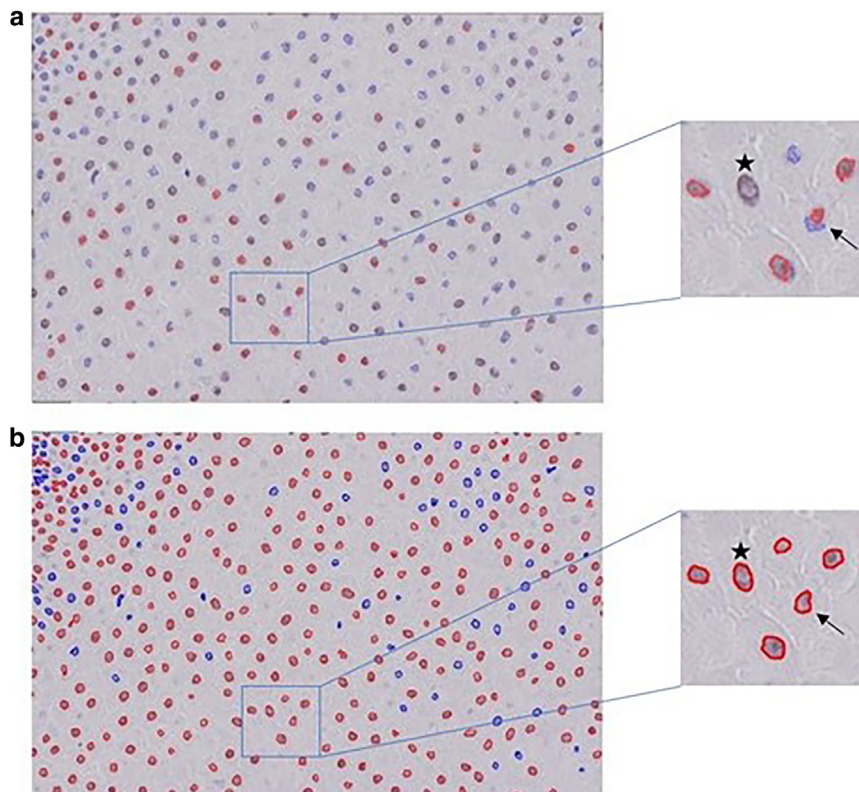
Samsung drive, an Intel UHD Graphics 750 graphics processing unit (GPU), and an NVIDIA is needed.

2. T1000 GPU: For efficient and timely handling of large images, a computer with large memory capacity and an advanced GPU is recommended but not required; a standard PC is capable of

running the program, albeit with increased time needed per operation.

3. Adobe Photoshop: Images used for this application were processed using Photoshop CC 2022.
4. Microsoft Office Excel.

Figure 6. Performance of QuPath versus SANDD in the region of interest from Figure 1. (a) QuPath. (b) SANDD. QuPath fails to detect some nuclei (star) and splits single nuclei into fragments, with inconsistent detection of positive staining (red vs blue rim) in fragments from a single nucleus (arrows). Bar = 100 μ m. SANDD, Standardized Algorithm for Nuclear Diaminobenzidine Detection.



Procedure

Preparation. Users proficient in coding may prefer to approach setup (package installation, environment handling, etc) using various other Python distributions, the Anaconda prompt, or a built-in command line. For novice users, the following instructions serve as a guide to equipping the computer to run the program.

On the computer(s) intended for use of this program, download and install a Python coding platform or integrated development environment (IDE). Anaconda (individual version 2022.05 used for development of this protocol) is recommended for user friendliness and the ability to create a sandbox or virtual environment in which packages are easily managed and minimal troubleshooting is required for users unfamiliar with coding. In addition to the Python 3 distribution provided by Anaconda, it can be used to install Python packages within environments.

In the Anaconda Navigator, create an environment using the Create button in the Environments tab, naming it as desired and selecting Python version 3.9.12. With the new environment selected, a search bar in the top right corner allows one to parse through available Python packages. Installation is only necessary upon first use, given that one is using the same environment for every session. Search the following terms and proceed with installation: Jupyterlab, Numpy, Opencv, and Matplotlib.

Selecting the green play button next to the environment name provides the option to open Jupyter Notebook within the environment and opens a new browser window resembling a Finder or File Manager window. Navigating to the directory in which a notebook file (such as the source code for this protocol) is located allows the option to open and fully interact with that notebook file.

Image preprocessing. Import images into Photoshop for isolation of the nucleated epidermis. Duplicate the background layer and hide the original layer for preservation of the original image in the case that starting over is needed. Using the eraser tool, remove all negative space surrounding the tissue section as well as dermis, endothelium, and cornified layers. Because overstaining can be anticipated on the perimeter of IHC sections, erasing these areas is also recommended. Folded areas or artifacts on the section may also be removed as needed, provided that the majority of keratinocyte nuclei are preserved with preference to the basal epidermis. The minimum number of nuclei used in testing this protocol was 2000. Once only the nucleated epidermis remains in the image, apply the Selective Color adjustment under Image > Adjustments. Navigate to the blue channel and set the yellow slider within the blue channel to -100 . This step enhances the hematoxylin counterstain and increases the contrast between the chromogen and hematoxylin.

Depending on the size of images generated by the microscope, image size can be increased proportional to the original size to increase the number of pixels per nucleus. The Preserve Details option for resampling as well as resolution control options in Photoshop maintain the image quality during resizing. Images used in testing were enlarged by doubling the number of pixels per inch and resampling with Preserve Details.

Crop the image so that the epidermis is bounded with minimal negative space. Save the image as a TIFF, ensuring run-length encoding layer compression, bit interleaved by pixel, and that no image compression options are selected. For ease of use, it is strongly recommended to save the images in the same directory or folder where the code file is located. It is also recommended to use short filenames that do not contain spaces and to document relationships between short and long identifiers as needed.

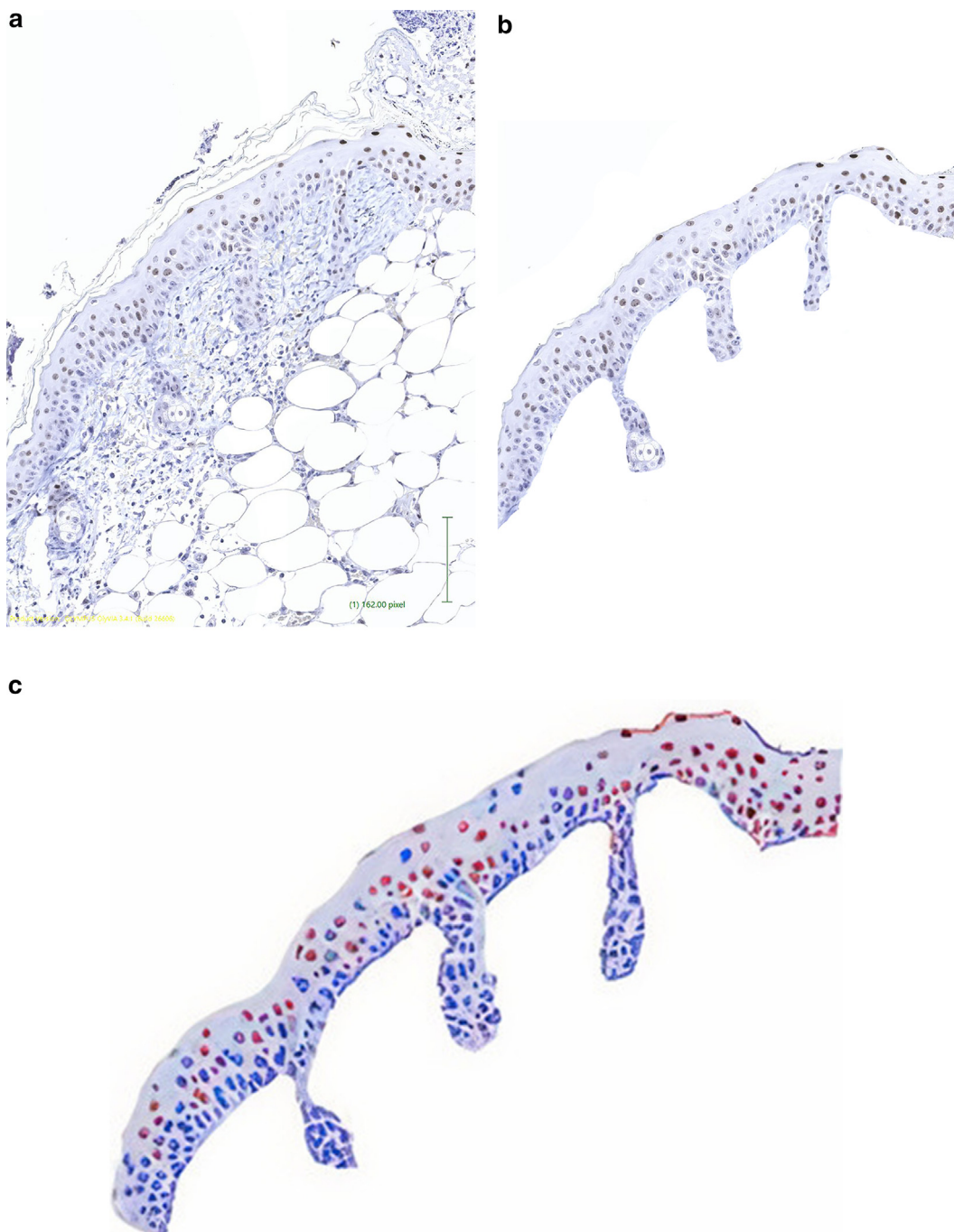


Figure 7. SANDD application to murine skin stained for phosphorylated c-Jun. (a) Original image of IHC-stained porcine skin. (b) Isolated epidermal segment produced in Photoshop. (c) Final image showing negative nuclei outlined in blue and positive nuclei outlined in red. Bar = 4286 μm. IHC, immunohistochemistry; SANDD, Standardized Algorithm for Nuclear Diaminobenzidine Detection.

To run the program, open the code file in Jupyter Notebook or the IDE of choice. In the final line of code, insert the name of the processed image file between the quotation marks so that the line reads the following: `runTotal('your_filename.tif')`. In the header bar, select the Run button. The program will print out information and export images throughout the run process that confirms that it is actively running as well as an asterisk (*) in the square brackets in the top left adjacent to the first line of the cell in Jupyter Notebook. On completion of the run, this asterisk is replaced with a number.

The result of the program will be a text printout of the counts of total, positive, and negative nuclei as well as an image with positive and negative nuclei outlined in red and blue, respectively.

The program outputs several images with the original filename as a prefix to prevent overwriting upon running the program multiple times. These images are located in the same directory as the original .tif file and code.

Troubleshooting. In the case of file not found or other missing data errors, ensure that all files (images and code) are located in the

Figure 8. QuPath application to porcine skin IHC stained for phosphorylated c-Jun. (a) Original image of IHC-stained porcine skin. (b) Final image showing negative nuclei outlined in blue and positive nuclei outlined in red. Bar = 4180 μ m. IHC, immunohistochemistry.

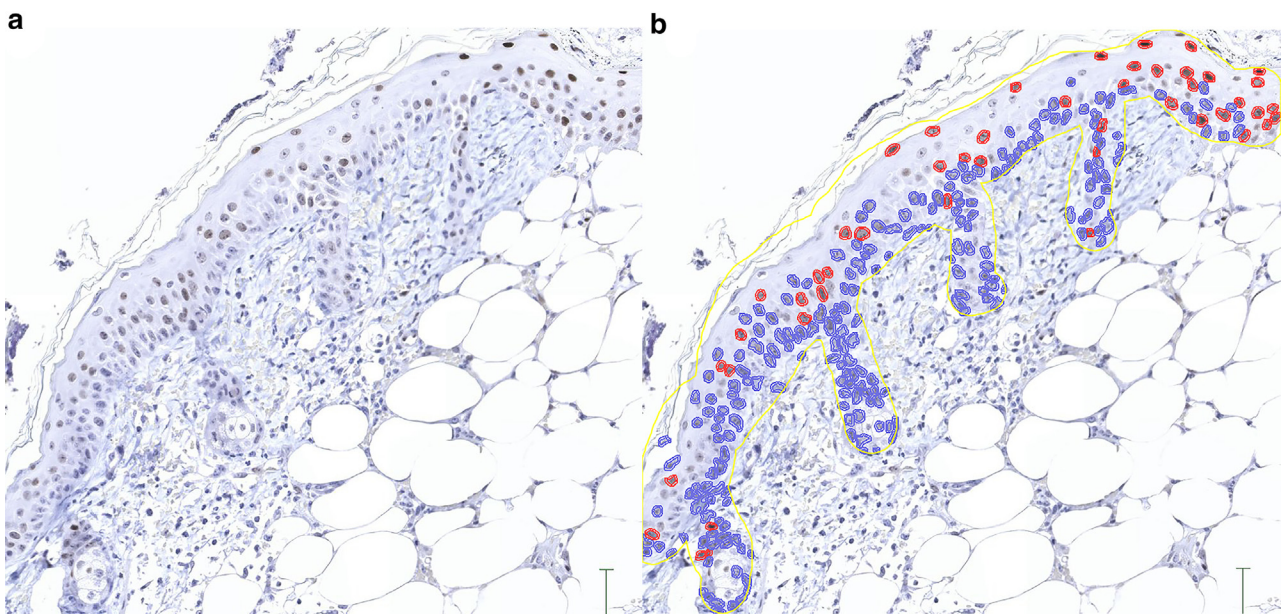
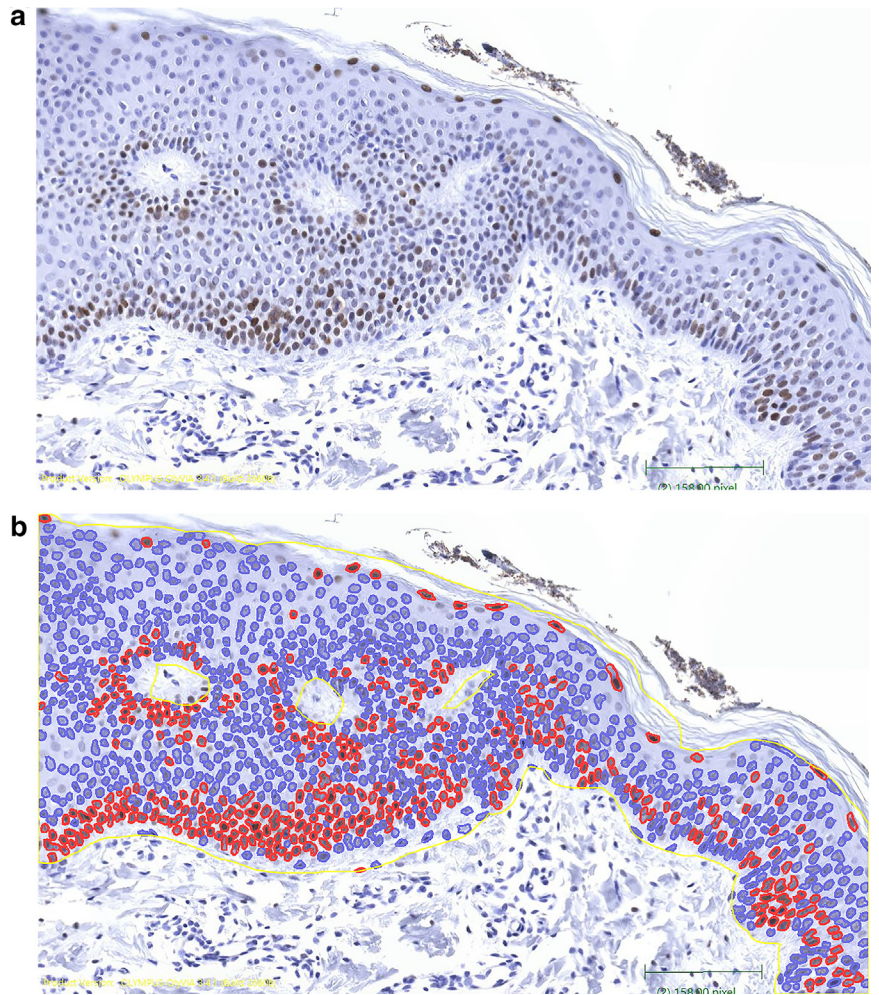


Figure 9. QuPath application to murine skin IHC stained for phosphorylated c-Jun. (a) Original image of IHC-stained murine skin. (b) Final image showing negative nuclei outlined in blue and positive nuclei outlined in red. Bar = 4286 μ m. IHC, immunohistochemistry.

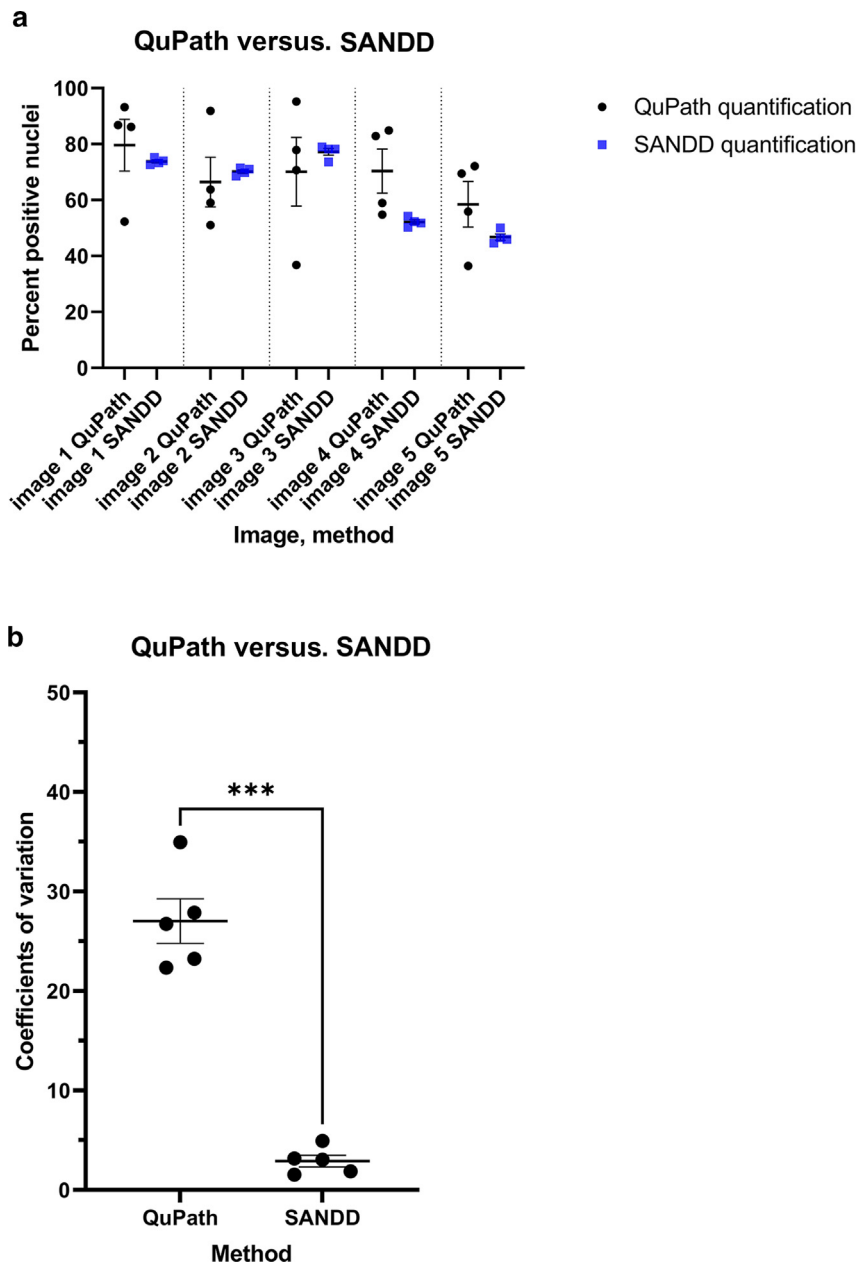


Figure 10. An improved method for quantification of nuclear biomarkers. (a) Comparison of QuPath with SANDD for percentage of positive keratinocytes stained for c-Myc in a set of 5 images, quantified by 4 observers. (b) Comparison of the coefficients of variation of quantifications (% positive nuclei) obtained by 4 observers analyzing images using QuPath versus SANDD. Data are expressed as mean \pm SEM for $n = 5$ images. $P = .008$ using 2-tailed paired t -test. SANDD, Standardized Algorithm for Nuclear Diaminobenzidine Detection.

same folder. Also, ensure that image filenames are entered into the code file exactly as saved.

In the case of package not found errors, check the Anaconda Navigator and ensure that all packages are installed within the environment being used. Additional Anaconda troubleshooting resources can be found at <https://docs.anaconda.com/anaconda/user-guide/troubleshooting/>.

Although the dataset used in developing this protocol cannot be made freely available, a set of images is available alongside the code in the GitHub repository for users to attempt the protocol before implementing into projects. Examples of the input and output files are also available.

Quality control. As mentioned earlier, the quirks of IHC require that staining undergo optimization and quality control prior to quantification. Ensuring that staining protocols are as standardized

as possible will produce the best quality images to analyze and will proactively reduce the amount of variability.

The export of images throughout the program run allows users to visually inspect the results. Some characteristics of keratinocyte differentiation may lead to improper segmentation, and in the case that a duplicate run is necessary, it is recommended that the image be reprocessed in Photoshop to remove problem areas. For example, beginning from the stratum granulosum, the cornification process alters nuclear morphology, appearing as broadly spread nuclei beginning to dissolve. Because the application of this program is specific to nuclear protein expression, intact nuclei are required. In addition, proteins that translocate from cytoplasm to nucleus or vice versa may not be accurately assessed.

Operations within this program can be optimized for desired applications. Nuclear size constraints, noise filtering, and the color calculation

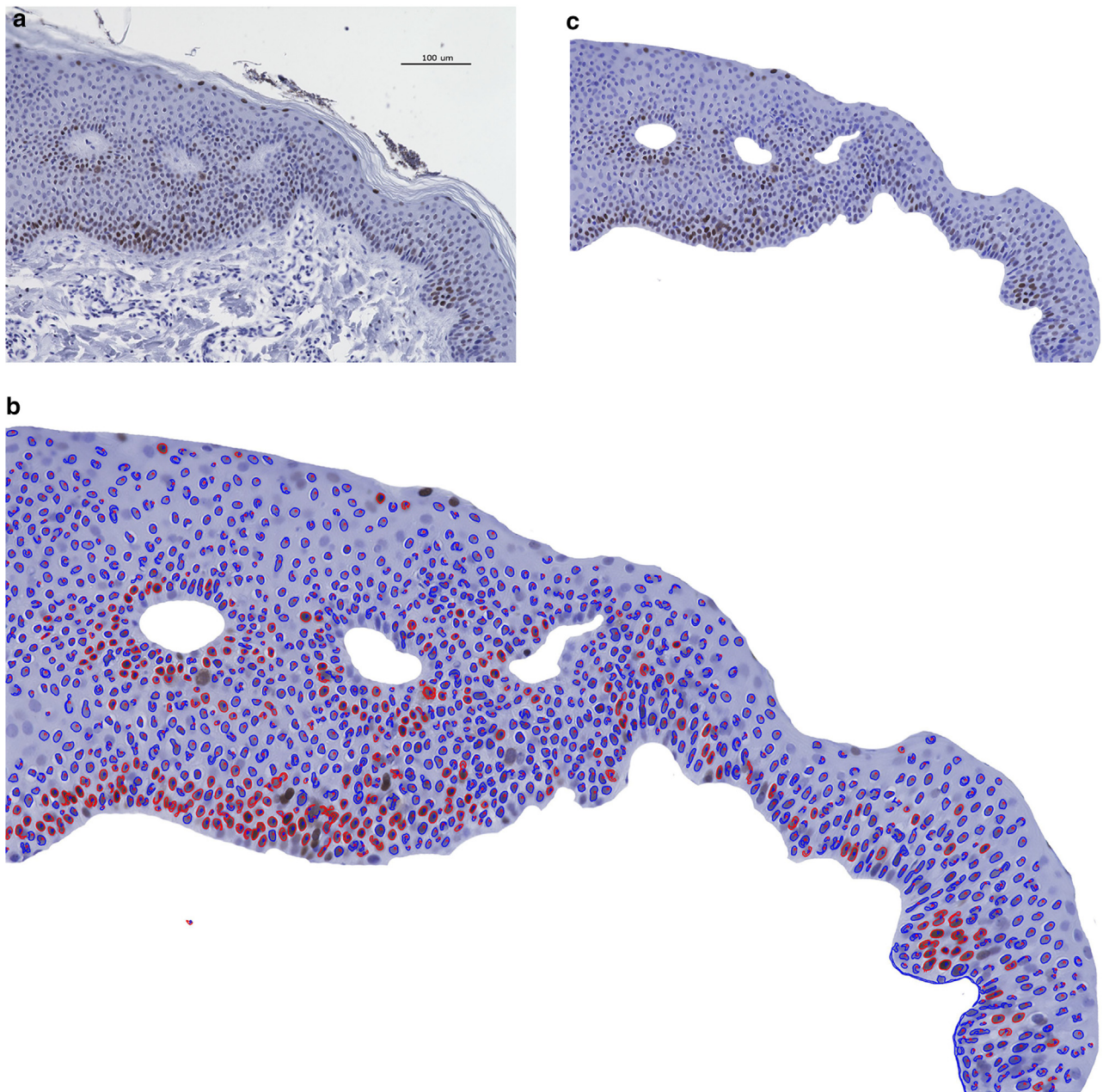


Figure 11. SANDD application to porcine skin IHC stained for phosphorylated c-Jun. (a) Original image of IHC-stained porcine skin. (b) Isolated epidermal segment produced in Photoshop. (c) Final image showing negative nuclei outlined in blue and positive nuclei outlined in red. Bar = 100 µm. IHC, immunohistochemistry; SANDD, Standardized Algorithm for Nuclear Diaminobenzidine Detection.

Table 3. Comparison of QuPath with SANDD for Percentage of Positive Keratinocytes Stained for Phosphorylated c-Junin Murine and Porcine Skin

Skin	QuPath			SANDD		
	Total Nuclei (Count)	Positive Nuclei (Count)	Positive Nuclei (%)	Total Nuclei (Count)	Positive Nuclei (Count)	Positive Nuclei (%)
Porcine skin	1291	427	33.08	1292	240	18.58
Murine skin	291	99	34.02	290	102	35.17

Abbreviation: SANDD, Standardized Algorithm for Nuclear Diaminobenzidine Detection.

itself are opportunities for modification depending on the needs of the group.

DATA AVAILABILITY STATEMENT

Datasets related to this article can be found at <https://github.com/lgsiegfried/SANDD>, hosted at Github repository.

ORCIDs

- Lindsey G. Siegfried: <http://orcid.org/0000-0002-6561-4113>
- Sophie M. Bilik <http://orcid.org/0000-0001-9370-6181>
- Jamie L. Burgess: <http://orcid.org/0000-0002-1137-6850>
- Paola Catanuto: <http://orcid.org/0000-0002-2157-9598>
- Ivan Jozic: <http://orcid.org/0000-0001-5114-9524>
- Irena Pastar: <http://orcid.org/0000-0003-0197-6198>
- Rivka C. Stone: <http://orcid.org/0000-0002-7489-2123>
- Marjana Tomic-Canic: <http://orcid.org/0000-0002-9341-0193>

CONFLICT OF INTEREST

The authors state no conflict of interest.

ACKNOWLEDGMENTS

We thank the National Institute of Diabetes and Digestive and Kidney Diseases Diabetic Foot Consortium for grant support U01DK119085 (MT-C), U24DK122927 (MT-C), U01DK119085 supplement (MT-C and RCS), and R61 DK131897 (RCS, MT-C) and for providing tissue samples used in this study. This work was also funded by the Dermatology Foundation Physician Scientist Career Development Award (RCS). We owe a debt of gratitude to late Carmen Perez, lead technician of the Dermatopathology Laboratory at the University of Miami Frost Dermatology for her commitment, dedication, and assistance in tissue processing. Marjana Tomic-Canic is the guarantor.

AUTHOR CONTRIBUTIONS

Conceptualization: LGS, RCS, MT-C; Data Curation: LGS, IP, RCS, MT-C; Formal Analysis: LGS, IP, RCS, MT-C; Funding Acquisition: RCS, MT-C; Investigation: LGS, SMB, PC, JLB, IP; Methodology: LGS, RCS, IP, MT-C; Project Administration: RCS, MT-C; Supervision: IP, RCS, MT-C; Validation: LGS, IP, RCS, MT-C; Visualization: LGS, SMB, JLB, IP, IP, RCS, MT-C; Writing - Original Draft Preparation: LGS, IP, RCS, MT-C; Writing - Review and Editing: LGS, SMB, JLB, IP, RCS, MT-C

DECLARATION OF GENERATIVE ARTIFICIAL INTELLIGENCE (AI) OR LARGE LANGUAGE MODELS (LLMs)

During the preparation of this work the author(s) did not use Generative Artificial Intelligence (AI) or Large Language Models (LLMs).

Disclaimer

The findings expressed are of the authors and may not reflect the views of the Diabetic Foot Consortium nor the National Institute of Diabetes and Digestive and Kidney Diseases.

REFERENCES

- Akakin H, Gokozan H, Otero J, Gurcan M. An adaptive algorithm for detection of multiple-type, positively stained nuclei in IHC images with minimal prior information: application to OLIG2 staining gliomas. Paper presented at: SPIE Medical Imaging. 2015; Orlando, FL.
- Anagnostou VK, Welsh AW, Giltneane JM, Siddiqui S, Liceaga C, Gustavson M, et al. Analytic variability in immunohistochemistry biomarker studies. *Cancer Epidemiol Biomarkers Prev* 2010;19:982–91.
- Bankhead P, Loughrey MB, Fernández JA, Dombrowski Y, McArt DG, Dunne PD, et al. QuPath: open source software for digital pathology image analysis. *Sci Rep* 2017;7:16878.
- Bradski G. The OpenCV Library. *Dr Dobbs J* 2000;25:120–5.
- Chen L, Bao J, Huang Q, Sun H. A robust and automated cell counting method in quantification of digital breast cancer immunohistochemistry images. *Pol J Pathol* 2019;70:162–73.
- Connolly C, Fleiss T. A study of efficiency and accuracy in the transformation from RGB to CIELAB color space. *IEEE Trans Image Process* 1997;6:1046–8.
- Cregger M, Berger AJ, Rimm DL. Immunohistochemistry and quantitative analysis of protein expression. *Arch Pathol Lab Med* 2006;130:1026–30.
- Crowe AR, Yue W. Semi-quantitative determination of protein expression using immunohistochemistry staining and analysis: an integrated protocol. *Bio Protoc* 2019;9:e3465.
- Di Cataldo S, Ficarra E, Acquaviva A, Macii E. Automated segmentation of tissue images for computerized IHC analysis. *Comput Methods Programs Biomed* 2010;100:1–15.
- Elliott K, McQuaid S, Salto-Tellez M, Maxwell P. Immunohistochemistry should undergo robust validation equivalent to that of molecular diagnostics. *J Clin Pathol* 2015;68:766–70.
- Engel KB, Moore HM. Effects of preanalytical variables on the detection of proteins by immunohistochemistry in formalin-fixed, paraffin-embedded tissue. *Arch Pathol Lab Med* 2011;135:537–43.
- Fernández-Carrobles MM, Bueno G, García-Rojo M, González-López L, López C, Déniz O. Automatic quantification of IHC stain in breast TMA using colour analysis. *Comput Med Imaging Graph* 2017;61:14–27.
- Fullerton A, Fischer T, Lahti A, Wilhelm KP, Takiwaki H, Serup J. Guidelines for measurement of skin colour and erythema. A report from the Standardization Group of the European Society of Contact Dermatitis. *Contact Dermatitis* 1996;35:1–10.
- Grube D. Constants and variables in immunohistochemistry. *Arch Histol Cytol* 2004;67:115–34.
- Guedes LB, Morais CL, Fedor H, Hicks J, Gurel B, Melamed J, et al. Effect of preanalytical variables on an automated PTEN immunohistochemistry assay for prostate cancer. *Arch Pathol Lab Med* 2019;143:338–48.
- Humphries MP, Maxwell P, Salto-Tellez M. QuPath: The global impact of an open source digital pathology system. *Comput Struct Biotechnol J* 2021;19:852–9.
- Janardhan KS, Jensen H, Clayton NP, Herbert RA. Immunohistochemistry in investigative and toxicologic pathology. *Toxicol Pathol* 2018;46:488–510.
- Libard S, Cerjan D, Alafuzoff I. Characteristics of the tissue section that influence the staining outcome in immunohistochemistry. *Histochem Cell Biol* 2019;151:91–6.
- Madabhushi A, Lee G. Image analysis and machine learning in digital pathology: challenges and opportunities. *Med Image Anal* 2016;33:170–5.
- Mendelsohn ML, Kolman WA, Perry B, Prewitt JM. Morphological analysis of cells and chromosomes by digital computer. *Methods Inf Med* 1965;4:163–7.
- Morris NJ, Conley GM, Ospina SM, Meehan WP Iii, Qiu J, Mannix R. Automated quantification of immunohistochemical staining of large animal brain tissue using QuPath software. *Neuroscience* 2020;429:235–44.
- Sawaya AP, Pastar I, Stojadinovic O, Lazovic S, Davis SC, Gil J, et al. Topical mevastatin promotes wound healing by inhibiting the transcription factor c-myc via the glucocorticoid receptor and the long non-coding RNA Gas5. *J Biol Chem* 2018;293:1439–49.
- Schneider CA, Rasband WS, Eliceiri KW. NIH Image to ImageJ: 25 years of image analysis. *Nat Methods* 2012;9:671–5.
- Seo H, Badieli Khuzani M, Vasudevan V, Huang C, Ren H, Xiao R, et al. Machine learning techniques for biomedical image segmentation: an overview of technical aspects and introduction to state-of-art applications. *Med Phys* 2020;47:e148–67.
- Stojadinovic O, Brem H, Vouthounis C, Lee B, Fallon J, Stallcup M, et al. Molecular pathogenesis of chronic wounds: the role of beta-catenin and c-myc in the inhibition of epithelialization and wound healing. *Am J Pathol* 2005;167:59–69.
- Stojadinovic O, Lee B, Vouthounis C, Vukelic S, Pastar I, Blumenberg M, et al. Novel genomic effects of glucocorticoids in epidermal keratinocytes: inhibition of apoptosis, interferon-gamma pathway, and wound healing along with promotion of terminal differentiation. *J Biol Chem* 2007;282:4021–34.
- Sukswai N, Khoury JD. Immunohistochemistry innovations for diagnosis and tissue-based biomarker detection. *Curr Hematol Malig Rep* 2019;14:368–75.
- Taylor CR, Levenson RM. Quantification of immunohistochemistry—issues concerning methods, utility and semiquantitative assessment II. *Histopathology* 2006;49:411–24.
- Valdebran M, Kowalski EH, Kneiber D, Li J, Kim J, Amber KT. Digital quantification of epidermal protein expression in paraffin-embedded tissue using immunohistochemistry. *Methods Mol Biol* 2020;2109:75–82.
- Varghese F, Bukhari AB, Malhotra R, De A. IHC Profiler: an open source plugin for the quantitative evaluation and automated scoring of immunohistochemistry images of human tissue samples. *PLoS One* 2014;9:e96801.
- Wang S, Yang DM, Rong R, Zhan X, Xiao G. Pathology image analysis using segmentation deep learning algorithms. *Am J Pathol* 2019;189:1686–98.
- Xu H, Mandal M. Epidermis segmentation in skin histopathological images based on thickness measurement and k-means algorithm. *EURASIP J Image Video Process* 2015;2015:18.



This work is licensed under a Creative Commons Attribution-NonCommercial-NoDerivatives 4.0 International License. To view a copy of this license, visit <http://creativecommons.org/licenses/by-nc-nd/4.0/>